Journal of Materials Chemistry C

Accepted Manuscript

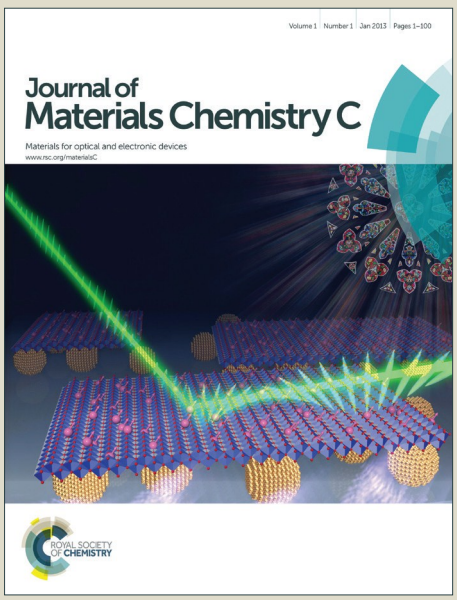

ROYAL SOCIETY OF CHEMISTRY

www.rsc.org/materialsC

Thioxanthene and Dioxothioxanthene Dihydroindeno[2,1-*b*]fluorenes : Synthesis, Properties and Applications in green and sky blue phosphorescent OLEDs†

Maxime Romain,[a] Cassandre Quinton,[a] Denis Tondelier,[b] Bernard Geffroy,[b,c] Olivier Jeannin,[a] Joëlle Rault-Berthelot*[a] and Cyril Poriel*[a]

Abstract. We report herein the synthesis, structural, electrochemical and photophysical properties of new dihydroindeno[2,1-*b*]fluorene-based semi-conductors, *i.e.* dispiro[thioxanthene-9,5'-indeno[2,1-*b*]fluorene-7',9"-thioxanthene] **2** and dispiro-[dioxothioxanthene-9,5'-indeno[2,1-*b*]fluorene-7',9"-thioxanthene] **3**. These properties will be compared to those of the pure hydrocarbon derivative dispiro[fluorene-9,5'-indeno[2,1-*b*]fluorene-7',9"-fluorene] **1** previously described. The incorporation of the sulfur atom within the bridged units allows to tune the HOMO and LUMO energy levels, retaining nevertheless the high E_T of the dihydroindeno[2,1-*b*]fluorenyl core ([2,1-*b*]IF), key feature for further device applications. This control of the properties has allowed incorporating **3** as host material in blue and green Phosphorescent OLEDs (PhOLED) with EQE of 12.8% (at 1 mA/cm^2 with corresponding CE and PE of 48.6 cd/A and 29.5 lm/W) for the green device and EQE of 4.8 % (at 1 mA/cm^2 with corresponding CE and PE of 14.8 cd/A and 8.2 lm/W) for the sky-blue device. To the best of our knowledge, this work is the second example of incorporation of a dihydroindeno[2,1-*b*]fluorene based semi-conductor in a blue PhOLED and highlights the potential of this fragment in organic electronics.

Introduction

Bridged terphenyls, so called dihydroindenofluorenes, have recently attracted particular attention due to their high potential in electronic applications.[1-3] Five positional isomers of dihydroindenofluorenes (Scheme 1-Top) have been thus reported to date in literature[1,2] and recent structure-properties relationship studies have shown the crucial importance (i) of the ring bridging (*syn/anti*)[1,3] and (ii) of the phenyl linkages (*ortho/meta/para*)[3] on their electronic properties. However, oppositely to the dihydroindeno[1,2-*b*]fluorenyl (*para anti* isomer) fragment which has been widely incorporated in many different electronic devices (organic light

*a. UMR CNRS 6226 "Institut des Sciences Chimiques de Rennes", Université de Rennes 1-Campus de Beaulieu-35042 Rennes cedex (France. *E-mail: cyril.poriel@univ-rennes1.fr, joelle.rault-berthelot@univ-rennes1.fr, Phone: (+33)2-2323-5977 or (+33)2-2323-5964*

b. UMR CNRS 7647, LPICM, CNRS, Ecole Polytechnique, Université Paris Saclay, 91128, Palaiseau, France

c. LICSEN, NIMBE, CEA, CNRS, Université Paris-Saclay, CEA Saclay 91191 Gif-sur-Yvette Cedex, France.

† Electronic supplementary information (ESI) available: Materials and methods and experimental details; synthesis and characterization of all compounds, theoretical modelling (DFT/TD-DFT), structural properties, thermal properties, Phosphorescent devices, copy of NMR spectra. CCDC 1435526 (molecule 2) and 1435527 (molecule 3).

emitting diodes-OLEDs-,[4-19] organic field effect transistors-OFETs-,[20-29] and organic solar cells [30-33]), the synthesis, the study and the incorporation in electronic devices of the other positional isomer derivatives, namely *meta anti* isomer [1,2-*a*],[3,34,35] *meta syn* isomer [2,1-*b*],[36] *para syn* isomer [2,1-*a*][37,38] and *ortho* isomer [2,1-*c*][3,39] have been very rarely reported. Their antiaromatic counterparts, namely indenofluorenes possessing a sp2 carbon atom at the bridges instead of a sp3 carbon atom, present very different properties and have also attracted remarkable attention in the last years.[22,40-43]

In this context, the *meta syn* isomer, *i.e.* dihydroindeno[2,1-*b*]-fluorene ([2,1-*b*]IF), has recently shown interesting performance in various electronic devices displaying its potential in organic electronics.[1,44,45] For example, a [2,1-*b*]IF-based semi-conductor substituted on the bridges with electron accepting dicyanovinylene units has been very recently incorporated in n-type OFETs with very promising performances and stability allowing their incorporations in an integrated circuit.[45] In addition, the first incorporation of a [2,1-*b*]IF derivative as emissive layer in non-doped blue OLEDs has been only reported in 2013 (molecule **1**, scheme 1-Bottom).[1] More recently, our groups have gone one step further, describing, through a strict control of the triplet state energy (E_T), the first incorporation of a dihydroindenofluorene isomer as host for blue triplet emitters in PhOLEDs.[3,36] Indeed, dihydroindenofluorenes with *para* or *ortho* linkages allow a good delocalization of π- electrons and hence possess low E_T (2.52 and 2.63 eV, respectively) not suitable to be used as host material for blue PhOLEDs. However, the *meta* linkages notably found in [2,1-*b*]IF reduces the π–conjugation, significantly increasing the E_T (2.76 eV) and keeping nevertheless excellent physical properties, crucial point for device performance and stability.[46] This wide range of electronic applications clearly highlights the versatility of this molecular fragment. Thus, the [2,1-*b*]IF core seems to have a brilliant future in organic electronics and it is hence of great importance to continue to design new semi-conductors based on this fragment. In this work, we wish to report two new semi-conductors based on the [2,1-*b*]IF scaffold and incorporating either thioxanthene units (TX), molecule **2**, or dioxothioxanthene units (TXO_2), molecule **3**, both spiroconjugated to the [2,1-*b*]IF core. TX is a structural analogue of xanthene, possessing an intracyclic sulfur atom instead of an oxygen atom. Recently, the potential of TX fragment has been shown in organic photovoltaic devices.[47] On the other hand, TXO_2 is the oxidized analogue of TX and the presence of the sulfone leads to a decrease of the Lowest Unoccupied Molecular Orbital (LUMO) level, which is beneficial for charge injection.[48-50] This particularity has been used to design active layers of electronic devices, either blue emitters for OLEDs[51-53] or host materials for PhOLEDs[49,50,54-56] or Thermally Activated Delayed Fluorescence (TADF) OLEDs.[57] However, the use of the TX/TXO_2 fragments remains scarce and we believe that these versatile systems deserve to be more deeply investigated.

Herein, we wish to report the synthesis, structural, electrochemical and photophysical properties of dispiro[thioxanthene-9,5'-indeno[2,1-*b*]fluorene-7',9''-thioxanthene] **2** and dispiro[dioxothio-xanthene-9,5'-indeno[2,1-*b*]fluorene-7',9''-thioxanthene] **3**, composed of TX or TXO_2/[2,1-*b*]IF association. Their properties will be compared to those of the known dispiro[fluorene-9,5'-indeno[2,1-*b*]fluorene-7',9''-fluorene] **1**, for which a new and regioselective synthetic access is described. Thus, the incorporation of the sulfur atom in such molecular structures allows the tuning of the Highest Occupied Molecular Orbital (HOMO) and LUMO energy levels, retaining nevertheless the high E_T of the [2,1-*b*]IF core, key feature for further electronic applications. Compound **3** has been finally incorporated as host material in green and blue PhOLEDs with

External Quantum Efficiency (EQE) of 12.8% (at 1 mA/cm^2) with corresponding Current Efficiency and PE of 48.6 cd/A and 29.5 lm/W for the green device and EQE of 4.8 % (at 1 mA/cm^2) with corresponding CE and PE of 14.8 cd/A and 8.2 lm/W for the sky-blue device.

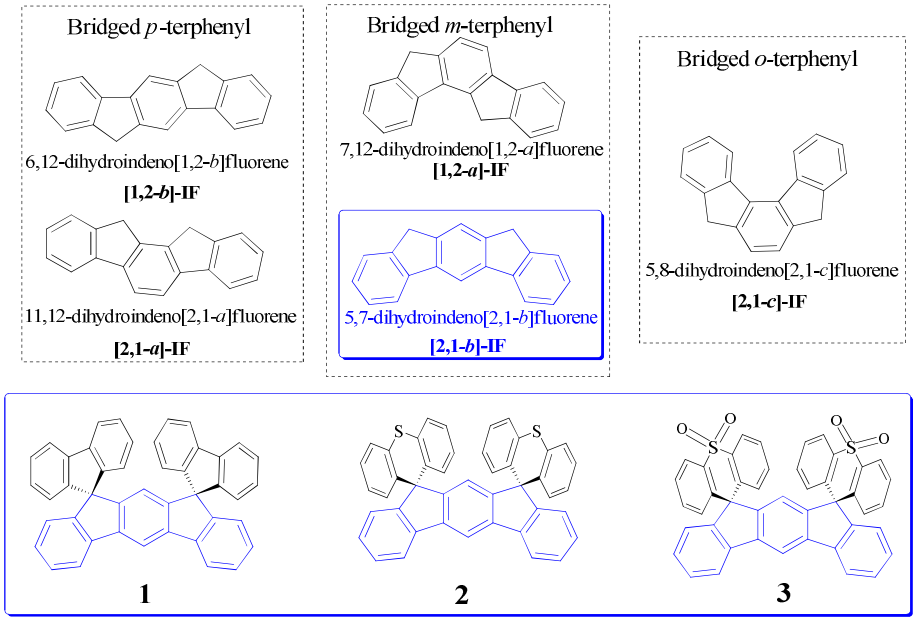

Scheme 1 The 5 dihydroindenofluorenes isomers (top) and the [2,1-*b*]-IF derivatives 1-3 investigated in this work (bottom).

Results and discussion

Synthetic Investigations

The synthesis of dihydroindeno[2,1-*b*]fluorene **1** has been recently reported.[1] The synthetic approach was based on an intramolecular electrophilic bicyclization reaction of a methoxy-fluorenol derivative leading to the formation of **1** together with its anti regioisomer dispiro[fluorene-9,12'-indeno[1,2-*a*]fluorene-7',9"-fluorene] (1/1 ratio) further separated by chromatography.[1] As the final isomers separation appears to be difficult, we started to investigate a new and regioselective route towards **1**, which presents the advantage of being also suitable for the synthesis of their thioxanthene (TX) and dioxothioxanthene (TXO_2) analogues **2** and **3** (Scheme 2). The key feature in this approach is to build up the [2,1-*b*]IF core prior to the final cyclization step in order to avoid isomers formation. This new approach is based on a coupling reaction between the key diketone **4**[45] possessing the [2,1-*b*]IF backbone in place with the 2-lithiumbiphenyl (Scheme 2-Bottom). The corresponding mixture of diastereoisomers of dihydroindenofluorenols is then cyclized in acid media to provide **1** with 60% yield. Similarly, the lithium halogen exchange of 2-iodophenyl-phenylsulfane **6**[50] (obtained from the amino analogue, 2-phenylthioaniline **5**) in presence of *n*-BuLi provides the lithiated derivative, further added to **4** to give the mixture of diols finally cyclised to provide **2**. Oxidation of the sulfur atoms of **2** in the presence of *meta*-chloroperbenzoic acid (mCPBA) provides the sulfone **3** with 96% yield. Thus, by a simple oxidation step, it is possible to modify the electronic effect of the sulfur atoms (see below) and hence to switch from electron donating to electron withdrawing properties, highlighting the versatility of these systems.

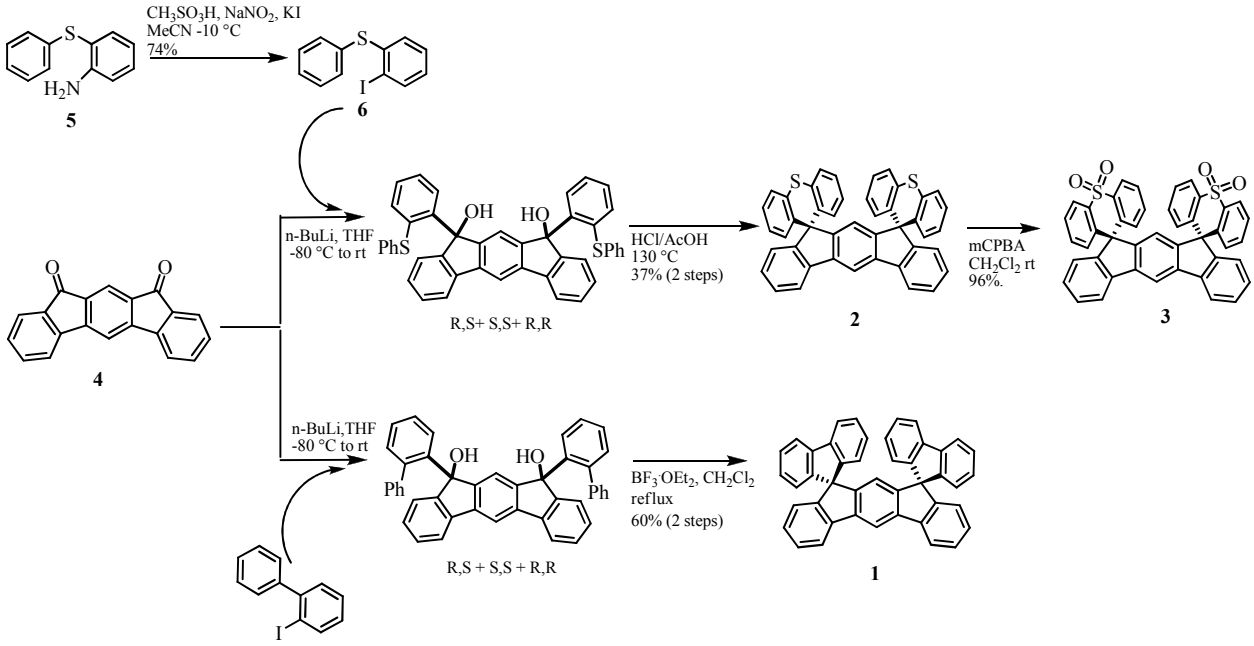

Scheme 2 Synthesis of the target molecules **1**, **2** and **3**.

^{1}H NMR Studies

Carefully analysing the hydrogens chemical shifts can be highly informative to evaluate the strength of the electron donating/withdrawing fragments on the surrounding hydrogens. Complete proton assignments of **1-3** have been performed by 2D NMR spectroscopy experiments (HMBC, HMQC and ^{1}H/^{1}H COSY, See SI). Thus, in ^{1}H NMR spectroscopy, we note that the signals of the dihydroindenofluorenyl core of **2** and **3** are found at different chemical shifts than those of its analogue **1** (Figure 1). More precisely, we note that the protons in α position of the spiro carbons, *i.e.* He (He of **2**: 7.7 ppm/ He of **3**: 7.6 ppm) and Hf (Hf of **2**: 7.4 ppm / Hf of **3**: 6.8 ppm) are strongly deshielded compared to those of **1** (He: 6.6 ppm / Hf: 6.1 ppm). In **1**, He and Hf are in the shielding cone of the orthogonal fluorenes and their resonances are detected at a high field. The replacement of the spiro-connected fluorenes in **1** by the spiro-connected TX/TXO$_2$ in **2** and **3** has important consequences on the surrounding hydrogen atoms through the displacement of the shielding cone. Thus, in **2** / **3**, the presence of the TX / TXO$_2$ unit and its central six-membered ring (*vs*. five-membered in the fluorene of **1**) erases this effect by displacing the shielding cone. In addition, we note the different electronic effect of the sulfur atom on the surrounding hydrogens as function of its oxidation degree. Indeed, the very different chemical shifts of the hydrogen atoms in α position of the thio-ether in **2** (Hg: 7.4 ppm) and of the sulfone in **3** (Hg: 8.1 ppm) clearly indicate the strong electron-withdrawing effect of the sulfone.

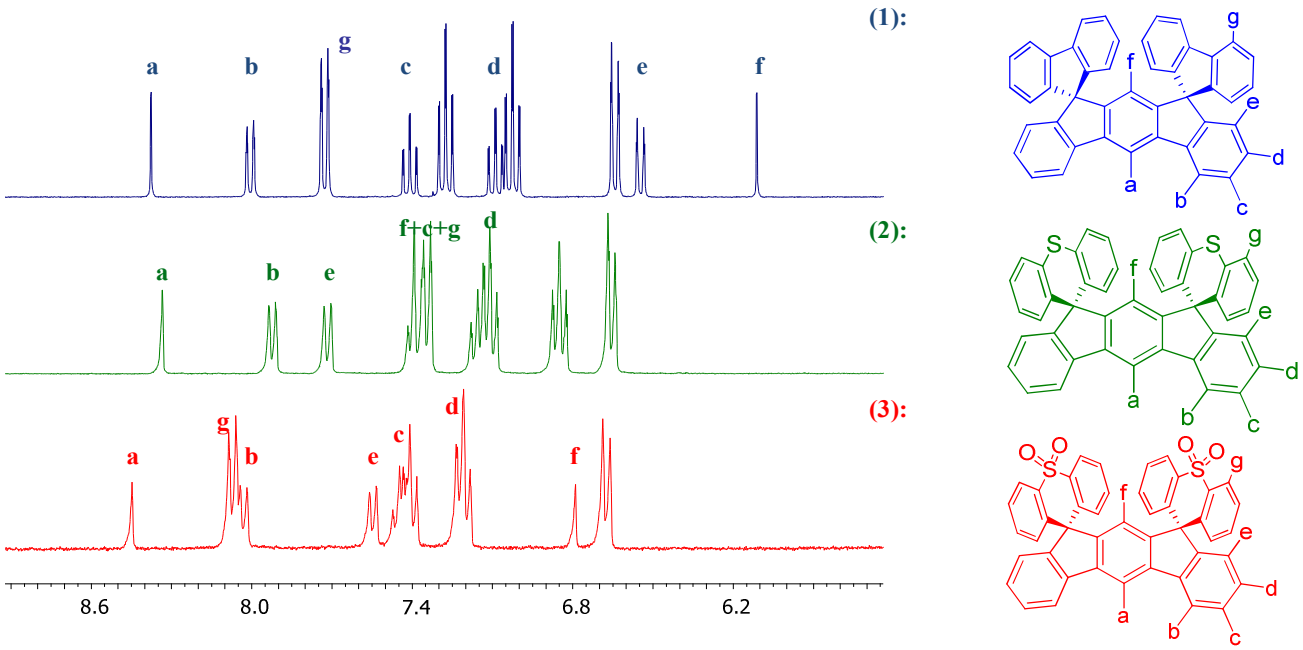

Figure 1. Portion of ^{1}H NMR spectra of **1** (Top), **2** (Middle) and **3** (Bottom) in CD_2Cl_2.

Structural Analyses

Molecular structures of **2** and **3** were further confirmed by X-ray crystallography on single crystal (vapour diffusion of pentane in a $CDCl_3$ solution), as shown in Figure 2. Thus, the X-ray diffraction data show that (i) **2** crystallises in the triclinic system, space group P-1, (ii) **3** crystallises with two molecules of $CDCl_3$ in the triclinic system, space group P-1 (see X-Rays in figure 2 and more details in SI). Molecular structure of **1** has been previously reported.[1]

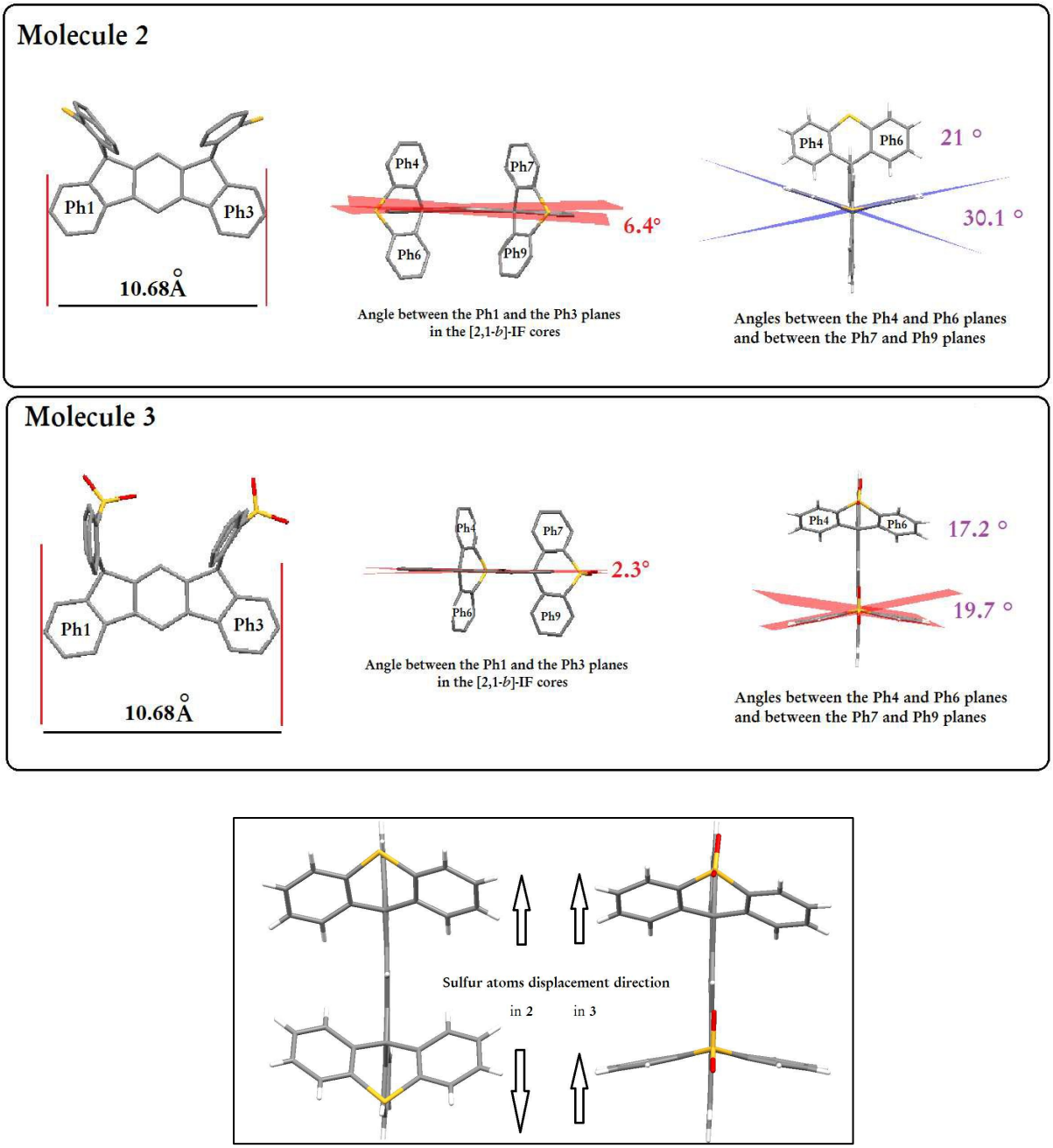

Figure 2 Molecular structures (capped sticks) from X-Ray crystallography of **2** (Top) and **3** (Middle), hydrogen atoms have been omitted for clarity. Curvature of TX units in **2** and of TXO_2 units in **3** (Bottom).

The [2,1-*b*]-IF core of **2** and **3** (Figure 2) has the same maximum length of 10.68 Å (distance between the two carbon atoms in β position of the bridge) almost identical to that of **1** (10.63 Å).[1] Accordingly, the [2,1-*b*]-IF core is contracted, due to its *meta* linkages, compared to the

other isomers with *para* linkages (11.1 Å[12] and 10.8 Å[58]). In addition, the [2,1-*b*]-IF core is not perfectly flat with a dihedral angle between the two side phenyl rings Ph1 and Ph3 of 6.4° in **2** and of 2.3° in **3**. Thus, in **2**, the [2,1-*b*]-IF core is more distorted than in **3**, for which the deformation is identical to that found in **1** (2.3°).[1] This feature is directly related to the rigidity of the substituents linked to the spiro bridges; the more rigid substituents, the less distorted [2,1-*b*]-IF core. Indeed, the tilt of the TX and TXO_2 units (angle between the mean planes of each phenyl unit, Ph4/Ph6 and Ph7/Ph9, in TX and TXO_2 units, Figure 2-Right) is measured at 21.0° and 30.1° for the TX units of **2** and at 17.2° and 19.7° for the TXO_2 units of **3**. It should be mentioned that the tilt of fluorenyl units is less than 2° in **1**, translating the high rigidity of the fluorene fragments. Thus, the TX units are more distorted and hence less rigid than the TXO_2 ones in accordance with the above mentioned conclusions on the [2,1-*b*]-IF deformation in **2** and **3**. It must be noted that in **3**, the two TXO_2 units are bent with the same curvature (with the two sulfur atoms shifting in the same direction) whereas in **2** the two TX units are bent in opposite direction (with the two sulfur atoms shifting in two opposite directions), Figure 2-Bottom.

Finally, in the packing diagram of **2**, a short C/S intermolecular distance is observed ($d_{C/S}$=3.495 Å, see SI). This distance is slightly shorter than the sum of the Van der Walls radii.[59] In addition, some short C/C intermolecular distances between two cofacial TX units are also detected ($d_{C/C=}$3.407 Å, $d_{C/C=}$3.451 Å, $d_{C/C=}$3.480 Å, see SI). These short distances translate the importance of the TX units in the solid state packing of **2**. Similarly, in the case of **3**, some short C/C intermolecular distances are also observed between TXO_2 units ($d_{C/C=}$3.456 Å, $d_{C/C=}$3.358 Å, see SI), with one being slightly shorter than the sum of the Van der alls radii.[59] In **3**, some significant short O-H contacts (inferior to the sum of the Van der Walls radii of O and H, ie 2.72 Å) involving the dihydroindenofluorene core and the sulfone have been also detected in the crystal packing (see SI).[59]

Optical properties

Absorption spectra of **2** (Figure 3-Left, green line) and **3** (Figure 3-Left, orange line) are very similar in shape and wavelengths to that of the pure hydrocarbon parent **1** (Figure 3-Left, blue line). All spectra display three main bands characteristic of the absorption of the [2,1-*b*]-IF core (344, 336 and 328 nm).[46] One can nevertheless note a small shift of 2 nm between the spectra of **2-3** and that of **1** highlighting a very small effect of the TX and TXO_2 units on the absorption of the [2,1-*b*]-IF core. However, at high energy, **2** and **3** do not present the intense band found at 310 nm in **1**, since this band reflect π-π* transitions located on the fluorenyl units.[12,60] Finally, optical gaps ΔE_{opt} (obtained from the onset of the last absorption band) have been all evaluated at ca 3.55 eV for the three derivatives.

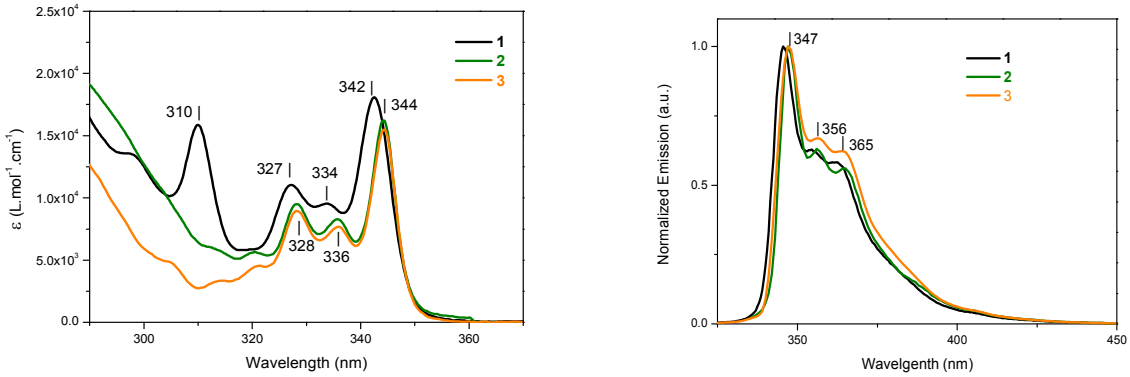

Figure 3 Left: UV-Vis Absorption, Right: emission (right, λ_{exc} = 300 nm, A (λ_{exc}) < 0.1 spectra of **1** (black line), **2** (green line) and **3** (orange line) in cyclohexane.

Quantum chemical calculations (Density Functional Theory, DFT, and Time Dependant DFT, TD-DFT) were carried out on **2** and **3**. TD-DFT calculations at the B3LYP level of theory with the 6-31+g(d) basis set were performed on the structures obtained by RX (see SI). For **3**, we first note that both HOMO and LUMO are localized on the [2,1-*b*]-IF core (Figure 4-Right) with no contribution of the TXO_2 fragment. From TD-DFT calculations, the main transition was detected as a HOMO/LUMO transition (f= 0.2281, λ_{th}=328 nm) involving only the [2,1-*b*]-IF core (Figure 4-Right). Compound **2** displays a different behaviour as the HOMO is localized on the TX unit and the LUMO on the [2,1-*b*]-IF fragment (Figure 4-Left). This leads to a disfavored through space HOMO/LUMO transition (λ=333 nm) possessing a weak oscillator strength of 0.0018. This is an important feature, which finds its origin in the HOMO/LUMO spatial separation (HOMO centered on the TX unit and LUMO on the [2,1-*b*]-IF core). The main transition of **2** appears hence as a HOMO-2/LUMO transition detected at λ_{th}=324 nm (f=0.2192) and involving only the [2,1-*b*]-IF fragment (Figure 5).

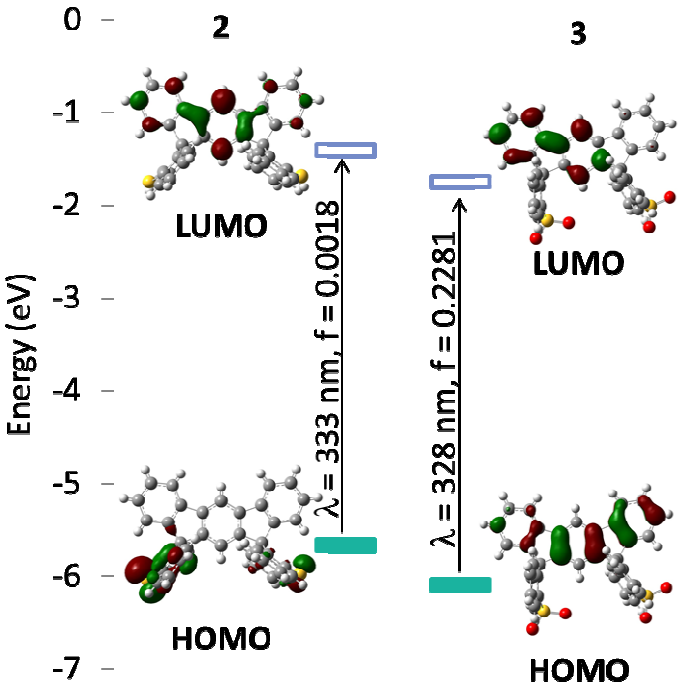

Figure 4 The HOMO→LUMO transition of **2** (Left) and **3** (Right) by TD-DFT with B3LYP/6-31+G(d), shown with an isovalue of 0.04 [e $bohr^{-3}$]$^{1/2}$

Thus, both compounds **2** and **3** show one experimental absorption band at ca. 344 nm (Figure 3-Left) which is due to a transition from the π_{IF} orbital centred on the [2,1-*b*]-IF core (HOMO-2 for **2** and HOMO for **3**) to the π^*_1 orbital LUMO also centred on the [2,1-*b*]-IF core (λ_{th}=324 and 328 nm, respectively for **2** and **3**, Figure 5). The significant overlap between the orbitals explains the intense absorption (molar absorption coefficients relative to this band (ε_{344nm}) are of 1.6×10^4 $L.mol^{-1}.cm^{-1}$ for both **2** and **3**, see SI) matching with a high theoretical oscillator strength (0.22 for **2** and 0.23 for **3**). Note that the occupied orbital involved in the main transition π_{IF} is the HOMO for **3** and the HOMO-2 for **2**, and thus ΔE_{opt} of **2** does not reflect the HOMO/LUMO difference.

The second absorption band experimentally found at ca. 336 nm (Figure 3-Left) is due in both cases to a transition from the π_{IF} orbital (HOMO-2 for **2** and HOMO for **3**) to the π^*_2 LUMO+1 (λ_{th}=301 and 311 nm, respectively for **2** and **3**, Figure 5). The third experimental absorption band of **2** and **3** localized at ca. 328 nm (Figure 3-Left) is due to two transitions for both compounds: the first one (λ_{th}=283 and 280 nm, respectively for **2** and **3**) from the π_{IF} orbital (HOMO-2 for **2** and HOMO for **3**) to the π^*_3 orbital localized on the left part of the molecule (both dihydroindenofluorene and TX/TXO_2, LUMO+2 for **2** and LUMO+5 for **3**) and the second one (λ_{th}=281 and 278 nm, respectively for **2** and **3**) from the π_{IF} orbital (HOMO-2 for **2** and HOMO for **3**) to the π^*_4 orbital localized on the right part of the molecule (both dihydroindenofluorene and TX/TXO_2, LUMO+3 for **2** and LUMO+6 for **3**). Thus, the almost identical absorption spectra of **2** and **3** are in perfect agreement with the similar calculated electronic transitions.

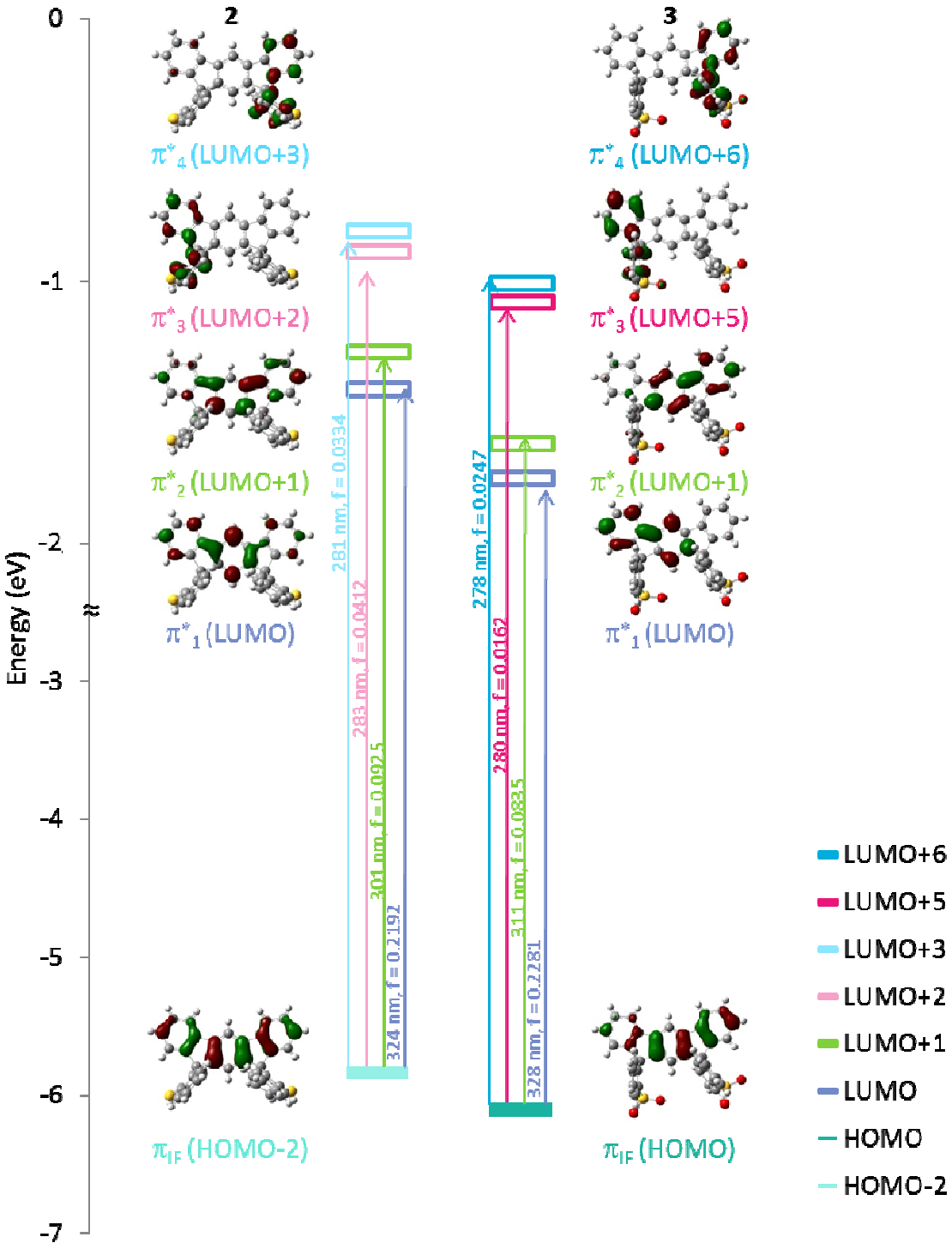

Figure 5 The 4th first main calculated electronic transitions of **2** (Left) and **3** (Right) by TD-DFT B3LYP/6-31+G(d), shown with a isovalue of 0.04 [e bohr^{-3}]$^{1/2}$.

In fluorescence spectroscopy in solution (Figure 3-Right), **2** and **3** present an almost identical emission spectrum in the near UV region with maxima at 347, 356 and 365 nm. As already observed in absorption spectroscopy, these spectra are almost identical to that of **1**,[36] translating

that the fluorescence properties in the three compounds directly arise from the [2,1-*b*]-IF core. In addition, **2** and **3** present a very small Stokes shift of 3 nm, translating very rigid molecular structures. This rigidity suppresses non radiative decay pathway providing the molecules a high quantum yield in solution (using quinine sulfate in sulfuric acid as a standard[61]), *i.e.* 0.57 for **2** and 0.44 for **3**. Thus, both the absorption and emission of **2** and **3** directly arise from the [2,1-*b*]-IF core with only very weak modifications due to the presence of TX and TXO_2 units.

Regarding the solid state fluorescence properties (Figure 6-Left), **2** and **3** both present an unresolved spectrum with a 19 nm red shift compared to their solution spectra. As this behaviour is clearly not observed in the case of **1**, one may conclude that TX (in **2**) and TXO_2 (in **3**) lead to stronger π–π intermolecular interactions in the solid state than the fluorene do (in **1**). This feature is surely assigned to the possible solid state structuration which can be done by the presence of the sulfur atom.

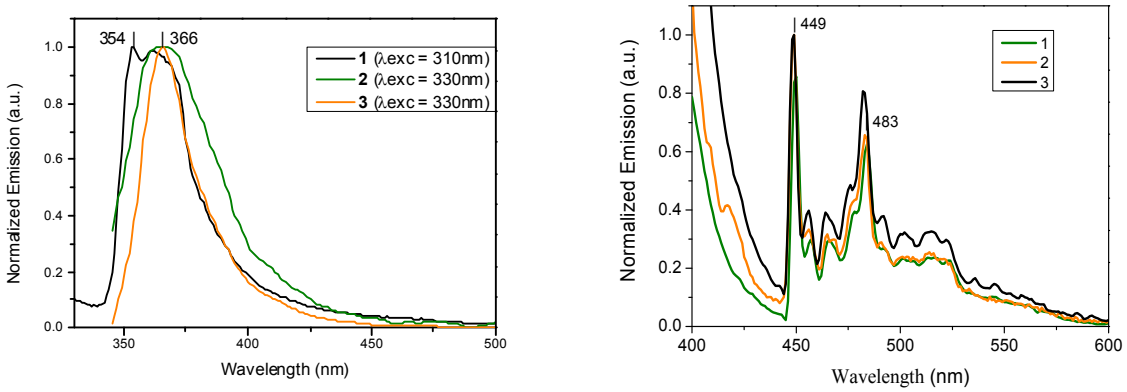

Figure 6 Left: Solid state emission in thin film (obtained from a THF solution at 10 mg/mL for **1** and **2** and at 3 mg/mL for **3**), Right: Emission spectra at 77 K of **1**, **2** and **3** (λ_{exc} = 300 nm, in 1:1 mixture of methylcyclohexane: 2-methylpentane for **1** and **2** and in 2-methyl THF for **3**).

The phosphorescence contribution of **1-3** can be observed on the emission spectra at 77 K (Figure 6-Right). Thus, **1-3** display well-resolved and similar phosphorescence spectra constituted of two thin bands with maxima at 449 and 483 nm (Figure 6-Right), blue shifted compared to those of *para* and *ortho* isomers of dihydroindefluorenes.[3] The corresponding E_T, obtained by the highest-energy phosphorescent peak, was evaluated at ca 2.76 eV for the three derivatives. Note that the E_T are theoretically calculated at 2.81, 2.82 and 2.77 eV for **1**, **2** and **3** respectively (Table 1) in accordance with experimental values. Thus, the identical E_T found for the three compounds indicate that the spiro-connected fragments (TX, TXO_2 or Fluorene) do not modify the E_T as a result of the π–conjugation reduction caused by the spiro carbons. However, these fragments will have an influence on the electrochemical properties of **1-3** as presented below.

Electrochemical Properties

Electrochemical behaviour of **2** and **3** has been studied by cyclic voltammetry and compared to that of **1**[1] (Figure 7, Table 1). Compounds **2** and **3** display a similar behaviour in oxidation (in dichloromethane, Figure 7-Left) with two irreversible waves at 1.43/1.89 V for **2** and 1.77/2.17

V for **3**. The reversibility of the first oxidation was observable only with a more than 2 V/s sweep-rate. Molecule **1** in identical experimental conditions also presents two oxidations waves at 1.53/1.93 V.[36] In light of electronic distribution of the HOMO (Figure 4) and the spin density of the cation radical of **2** and **3** (Figure 8), the first electron transfer of **2** and **3** seems to be differently centred. Indeed, in the case of **3**, the first oxidation seems to be centred on the longer π–conjugated fragment, *i.e.* dihydroindenofluorene as also observed for **1**.[1] Thus, the electron-withdrawing effect of the TXO_2 units shifts to more anodic potentials the oxidation of the [2,1-*b*]-IF core. Due to that, the HOMO level of **3**, determined from the onset oxidation potential[62] is deep (-6.04 eV), and lower than that of **1** (-5.80 eV). In the case of **2**, the situation appears different as in light of the electronic distribution of the HOMO (Figure 4) and the spin density of the cation radical (Figure 8), the first electron transfer seems to be centred on the TX unit. The HOMO level of **2** (-5.71 eV) is hence higher in energy than that of **3** (-6.04 eV) and closed to that of **1** (-5.80 eV). Note that this trend of HOMO energy levels is in accordance with that found through theoretical calculations (the HOMO of **3**, -6.10 eV, is deeper than those of both **1**, -5.60 eV, and **2**, -5.66 eV, which are very close one to the other others). It should be stressed that other dyes incorporating TX units spirolinked to either TXO_2 or diazafluorene fragments have been recently reported by our groups with HOMO levels lying at -5.79 and -5.70 eV respectively (oxidation centred on the TX unit),[50] being hence in accordance with the present work. However, as the HOMO level of **1** is also very close (-5.80 eV, oxidation of the [2,1-*b*]-IF core), it is important to mention that it is difficult to assign with a complete certitude this first electron transfer in **2**. Moreover, one may point that neither **2** nor **3** oxidations even reaching high potential values lead to electropolymerization processes (as observed for **1** by the intense cathodic current at the reverse sweep).

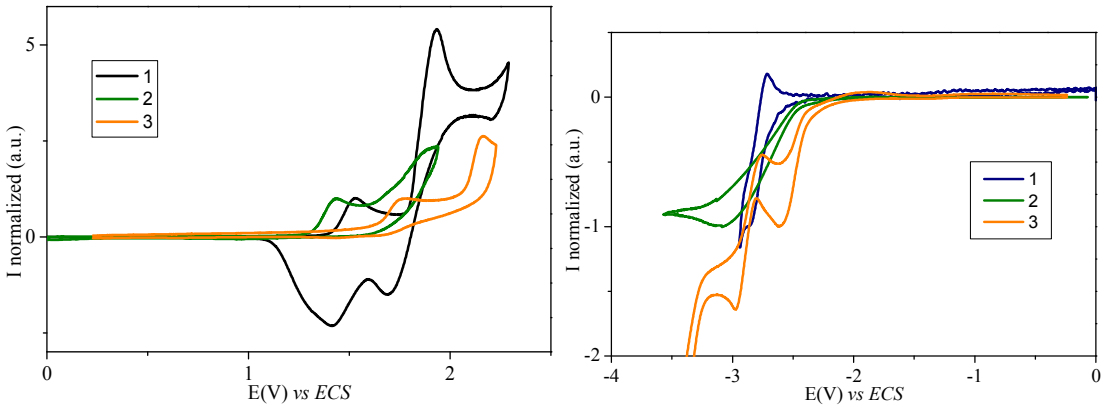

Figure 7 Cyclic voltammetry at 100 mV/s of **1** (3×10^{-3} M), **2** (3×10^{-3} M) and 3 ($<3\times10^{-3}$ M). Left: in oxidation in CH_2Cl_2/$[Bu_4N][PF_6]$ 0.2 M. Right: in reduction in THF/$[Bu_4N][PF_6]$ 0.2 M. A platinum disk is used as a working electrode (diameter 1 mm). For the 3 compounds the intensity is normalized at the first oxidation or reduction wave.

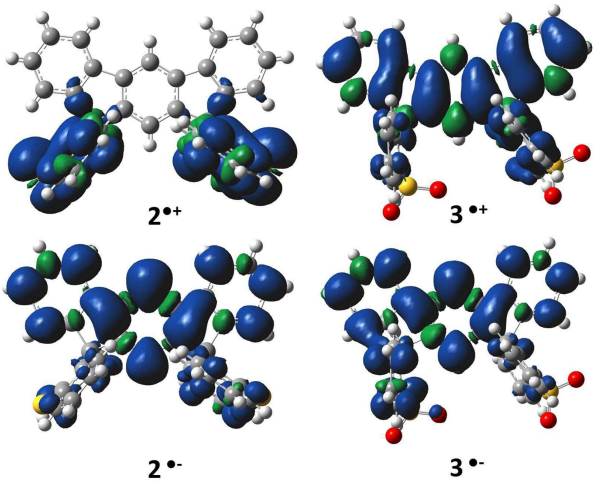

Figure 8 Spin density of the cation radical (Top) and of the anion radical (Bottom) of **2** (Left) and **3** (Right) shown with an isovalue of 0.04 [e bohr^{-3}]$^{1/2}$.

In the cathodic range (in THF, Figure 7-Right), **2** presents an irreversible reduction wave with a maximum at -3.10 V. Due to the presence of the electrowithdrawing sulfone, the first reduction of **3** is significantly shifted to -2.56 V and a second wave is even observed with a maximum at -2.96 V. In light of electronic density of LUMO and the spin density of the anion radical of **2** and **3**, the reduction of **2** and **3** seems to be centred on the [2,1-*b*]-IF as previously also observed for **1**. This is a different result than that observed for oxidation. Compared to **1**, which possesses a first reduction at -2.84 V, one can hence note that the TXO_2 unit renders the [2,1-*b*]-IF core more easily reducible in accordance with the above mentioned conclusions in oxidation. In the case of **2**, as the reduction wave is broad and therefore cannot correspond to a simple one or two electron process, the comparison of the potentials appears difficult. The LUMO of **2** and **3** determined from the onset reduction potentials,[62] were respectively evaluated at -1.98 and -2.06 eV, significantly decrease compared to that of **1** (-1.75 eV). Thanks to theoretical calculations, LUMO levels were calculated at -1.21, -1.41 and -1.75 eV for **1**, **2** and **3**, keeping the same trend than that exposed above through electrochemical data. Finally, the electrochemical gaps (ΔE_{El}, Table 1) of **1-3** are wide and evaluated at 4.05, 3.70 eV and 3.98 eV respectively. Note that the same trend is found by theoretical calculations (4.39, 4.25 and 4.35 eV for **1-3** respectively)

Table 1 Optical and Electrochemical properties of **1**, **2** and **3**: wavelength λ (in nm), molar absorption coefficient ε (in $L.mol^{-1}.cm^{-1}$), energy gap ΔE (in eV), fluorescent quantum yield ϕ (in %, λ_{exc} = 310 nm),peak potential E (in V *vs* SCE), triplet state energy E_T (in eV)

	λ_{ABS} $[10^4.\varepsilon]^a$	$\lambda_{EM}{}^a$	$\lambda_{EM}{}^b$	$\Delta E_{opt}{}^c$	$\Delta\nu^{a,h}$	Φ^a	E_{Texp}	Eox^f	HOMO exp	$Ered^g$	LUMO exp	ΔE_{El}	HOMO theo	LUMO theo	ΔE_{th}	E_{Tth}
	nm	nm	nm	eV	cm^{-1}	%	eV	V	eV	V	eV	eV	eV	eV	eV	eV
1[3]	342*[1.8] 334 [1.0] 327 [1.1] 310 [1.6]	346* 354 362	354* 362	3.55	338	51	2.76[d]	1.53 1.93	-5.80	-2.84	-1.75	4.05	-5.60	-1.21	4.39	2.81
2	344*[1.6] 336 [0.9] 328 [1.0] 320 [0.6]	347* 356 365	366*	3.55	251	57	2.76[d]	1.43 1.89	-5.71	-3.10	-1.98	3.70	-5.66	-1.41	4.25	2.82
3	344*[1.6] 336 [0.8] 328 [0.9] 320 [0.5]	347* 356 365	366*	3.55	251	44	2.76[e]	1.77 2.17	-6.04	-2.56 -2.96	-2.06	3.98	-6.10	-1.75	4.35	2.77

a\ in cyclohexane, **b**\ in thin film (obtained by spin-coating from a THF solution at 10mg/mL for **1** and **2** and at 3mg/mL for **3**), **c**\, determined with the onset absorption at λ_{ABS}=349 nm (ΔE^{opt} (eV) = 1239.84/ λ (in nm)) **d**\ in 1/1 methylcyclohexane/2-methylpentane **e**\ in 2-MeTHF, **f**\in CH_2Cl_2, **g**\ in THF , **h**\Stokes shift: $\Delta\nu\ (cm^{-1}) = 10^7(1/\lambda_{max\text{-}ABS\ (in\ nm)} - 1/\lambda_{max\text{-}EM\ (in\ nm)})$, ***** λmax.

Phosphorescent Organic Light Emitting Diodes

Finally, PhOLEDs using either the green dopant, fac-tris[2-phenylpyridinato-C^2,N]iridium(III) ($Ir(ppy)_3$) or the sky blue dopant, Bis[2-(4,6-difluorophenyl)pyridinato-C^2,N](picolinato)iridium(III) (FIrpic) and **3** as host have been fabricated, characterized and their performances have been compared to those of the pure hydrocarbon **1** (Table 2). As we have previously shown that host materials incorporating TX units lead to poor device performance[49,50] whereas those incorporating TXO_2 fragment lead to high performances, only **3** has been incorporated as host in green and sky blue PhOLEDs. The PhOLED structure is ITO/CuPc (10 nm)/NPB (40 nm)/TCTA (10 nm)/EML:dopant (20 nm)/TPBi (40 nm)/LiF (1.2 nm)/Al (100 nm). Indium Tin oxide (ITO) is the anode, copper phtalocyanine (CuPc) is the hole injecting layer, *N*,*N'*-di(1-naphtyl)-*N*,*N'*-diphenyl-[1,1'-biphenyl]-4,4'-diamine (NPB) is the hole-transporting layer, 4,4',4"-tris(carbazol-9-yl)-triphenylamine (TCTA) is the electron/exciton blocking layer, 1,3,5-tris(1-phenyl-1H-benzimidazol-2-yl)benzene (TPBI) is both the electron

transporting layer and the hole blocking layer and lithium fluoride covered with aluminum is the cathode.

As stated in the introduction, the performance of **1** has been previously reported.[3] For an accurate performance comparison, for each device, the threshold voltage (V_{th}) is measured for a luminance of 1 cd/m^2, the current and power efficiencies (CE and PE) are reported at 1 and 10 mA/cm^2 and the external quantum efficiency (EQE) is calculated at 1 and 10 mA/cm^2 (Table 2). Performance at 100 cd/m^2 and more importantly at the high luminance of 1000 cd/m^2 is reported in SI. First, green PhOLEDs using **3** as host possess EQE of 12.8% at 1 mA/cm^2 with corresponding CE and PE of 48.6 cd/A and 29.5 lm/W (Figure 9, Table 2). To properly compare the efficiency of a host material in a PhOLED, the device architecture should be identical. As our groups have recently reported other green phosphorescent devices with the same configuration than that used herein [‡] but using different host materials based on small molecular units, the direct comparison of the host efficiency is possible. Thus, the performance of various green PhOLEDs using as host either spirobifluorene (EQE=8.4%),[60] 4-phenylspirobifluorene (EQE=10.6%),[60] 4-pyridylspirobifluorene (different pyridine isomers with EQE varying between 12.7 and 15.7 %),[63] 4,5-pyrimidylspirobifluorene (13.8%)[63] have been reported. One can hence note that the present host **3** displays better performance than those of spirobifluorene and 4-phenylspirobifluorene but lower than those incorporating pyridines and pyrimidine, which are good electron transporting units. This is a promising feature for the future of dihydroindenofluorene derivatives.

For comparison purpose, it should be mentioned that pure hydrocarbon **1** displays a slightly higher EQE of 14.5 % at 1 mA/cm^2 with corresponding CE and PE of 58.3 cd/A and 28.3 lm/W (Table 2).[36] We nevertheless note that Von is decreased from 3.7 for **1** to 3.2 V for **3**, surely due to the decrease of the LUMO level of **3**, which favours the electron injection in the host. Thus, compound **3** displays equivalent performance to that of **1** with the beneficial effect of the LUMO lowering which lead to lower Von.

At high luminance (see Table in SI), we note that the performance of **3** remains high with an EQE of 12.4 % at 1000 cd/m^2 with corresponding CE of 52.2 and 47 cd/A (13.8% at 100 cd/m^2).

The electroluminescent (EL) spectrum of **3**-based PhOLED (Figure 10, green line) displays the emission maxima of the green dopant Ir(ppy)$_3$ at 516/540 nm (CIE coordinates: (0.33; 0.62)) in accordance with the emission of the pure Ir(ppy)$_3$ (509/540 nm).[64]

[‡] Indeed, the present device architecture has been previously used by our groups with many other hosts allowing hence the direct comparison of the host efficiency. This a key feature to precisely define structure-properties relationships.

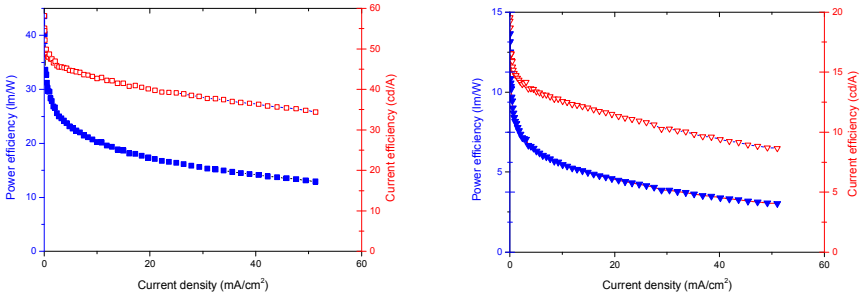

Figure 9 Current (cd/A, red symbols) and Power (lm/W, blue symbols) Efficiencies *vs* Current Density (mA/cm^2) for green (left, Irppy$_3$-10 wt%) and blue (right, FIrpic-20 wt%) devices using **3** as host (blue line).

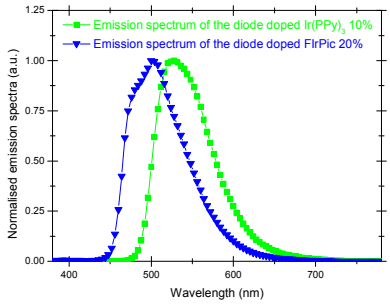

Figure 10 EL spectra of green (Irppy$_3$, 10 wt%, black line) and sky blue (FIrpic, blue line) devices

Compound **3** has finally been incorporated as host in sky blue PhOLEDs (FIrpic, E_T: 2.62 eV[65]). Thus, PhOLEDs using **3** as host present at 1 mA/cm^2 an EQE of 4.8% with corresponding CE and PE of 14.8 cd/A and 8.2 lm/W (Table 2, Figure 9-Right). These performances are comparable to those reported for the spirobifluorenes based host described above (EQE comprised between 3.9 and 6.0%) with a similar device structure.[60,63] Although not very high, the performance of **3**-based blue devices is similar to that reported for **1** (EQE of 5.3% at 1 mA/cm^2, with corresponding CE and PE of 14.7 cd/A and 8.3 lm/W) and confirms the possibility to use dihydroindenofluorenes as host for sky blue PhOLEDs. Indeed, most of the time efficient devices are obtained with short molecular fragments (2 bridged phenyl units) as host[66] and the present devices using a longer π–conjugated molecule (3 bridged phenyl units in dihydroindenofluorenes) as host are hence very interesting from this point of view. We believe that with a judicious further molecular design such semi-conductors may lead to strongly enhanced performance.

As observed for the green devices (see above), we note that the performance of **3** remains stable at a luminance of 100 cd/m^2 and slightly decrease at 1000 cd/m^2 (see Table in SI).

EL spectra of blue devices (Figure 10, blue line) reveal the emission of the sky blue dopant FIrpic with maxima at 473 and 500 nm (CIE: 0.20; 0.47) in perfect accordance with the emission of the pure FIrpic film (475/500 nm).[67,65] However, the relative intensity of the two peaks is

inverted in our device (intensity of the peak at 500 nm is higher than that of 473 nm) with respect to other reported works. Optical effects taking place within the multilayer structure could explain this result as it has been reported in the literature.[68,69] One can note, that there is no residual emission notably arising from the host, signing good host/guest energy transfers.

Table 2. Performance of green ($Ir(ppy)_3$) and sky blue (FIrpic) devices.

EML	Von (V)	CE (cd/A)		PE (lm/W)		EQE (%)		CIE (x;y)
	L=1[a]	J=1[b]	J=10[b]	J=1[b]	J=10[b]	J=1[b]	J=10[b]	J=10[b]
	$Ir(ppy)_3$ based devices (10 wt %)							
1	3.7	58.3	49.6	28.3	18.5	14.5	12.3	0.32; 0.62
3	3.2	48.6	42.7	29.5	20.3	12.8	11.3	0.33; 0.62
	FIrpic based devices (20 wt %)							
1	3.9	14.7	13.6	8.3	6.0	5.3	4.9	0.20; 0.44
3	3.9	14.8	12.6	8.2	5.6	4.8	4.1	0.20; 0.47

(**a**\ in cd/m², **b**\ in mA/cm²)

Conclusion

In summary, we have reported new semi-conductors based on the dihydroindeno[2,1-*b*]fluorenyl fragment and incorporating TX and TXO_2 units. The incorporation of the sulfur atoms leads to a tuning of the HOMO/LUMO energy levels, retaining the high E_T of the dihydroindeno[2,1-*b*]fluorenyl core, key feature for green and blue PhOLED applications. Molecule **3** has been incorporated as host material in blue and green Phosphorescent OLEDs (PhOLED) with EQE of 12.8 % (at 1 mA/cm^2 corresponding CE and PE of 48.6 cd/A and 29.5 lm/W) for the green device and EQE of 4.8 % (at 1 mA/cm^2 corresponding CE and PE of 14.8 cd/A and 8.2 lm/W) for the sky-blue device. These performances are almost identical compare to those of its pure hydrocarbon **1** with nevertheless a lower Von for the green devices due to better charge injection. With a more judicious molecular design, we believe that the performance of such dihydroindeno[2,1-*b*]fluorene compounds can be strongly enhanced highlighting the potential of this versatile fragment in organic electronics.

Acknowledgment

We wish to thank the ANR (Project *"Men In Blue"* n° ANR-14-CE05-0024) for financial support and for a post doctoral grant (CQ), the CDIFX (Rennes) for X-Ray diffraction data, the C.R.M.P.O for mass analysis, Dr F. Barrière (Rennes) and the GENCI (c2015085032) for computing time, the Institut des Sciences Analytiques (Villeurbanne) for TGA, the Service de Microanalyse-CNRS (Gif sur Yvette) for CHN analyses, the region Bretagne and the ADEME

for a studentship (MR), Dr B. Laffite (ADEME), S. Fryars (Rennes) for invaluable technical assistance.

References

1 M. Romain, D. Tondelier, J.-C. Vanel, B. Geffroy, O. Jeannin, J. Rault-Berthelot, R. Métivier, C. Poriel, *Angew. Chem. Int. Ed.* 2013, **52**, 14147-14151.
2 A. G. Fix, D. T. Chase, M. M. Haley, in *Top. Curr. Chem* (Eds.: J. S. Siegel, Y.-T. Wu), Springer-Verlag Berlin Heidelberg, **2014**, pp. 159-195.
3 M. Romain, S. Thiery, A. Shirinskaya, C. Declairieux, D. Tondelier, B. Geffroy, O. Jeannin, J. Rault-Berthelot, R. Métivier, C. Poriel, *Angew. Chem. Int. Ed.* 2015, **54**, 1176-1180.
4 S. Becker, C. Ego, A. C. Grimsdale, E. J. W. List, D. Marsitzky, A. Pogantsch, S. Setayesh, G. Leising, K. Müllen, *Synth. Met.* 2002, **125**, 73-80.
5 A. C. Grimsdale, K. Müllen, *Macromol. Rapid. Commun.* 2007, **28**, 1676-1702.
6 A. C. Grimsdale, K. L. Chan, R. E. Martin, P. G. Jokisz, A. B. Holmes, *Chem. Rev.* 2009, **109**, 897–1091.
7 J. Jacob, J. Zhang, A. C. Grimsdale, K. Müllen, M. Gaal, E. J. W. List, *Macromolecules* 2003, **36**, 8240-8245.
8 Y. Park, J.-H. Lee, D. H. Jung, S.-H. Liu, Y.-H. Lin, L.-Y. Chen, C.-C. Wu, J. Park, *J. Mater. Chem.* 2010, **20**, 5930-5936.
9 D. Thirion, J. Rault-Berthelot, L. Vignau, C. Poriel, *Org. Lett.* 2011, **13**, 4418-4421.
10 D. Marsitzky, J. C. Scott, J.-P. Chen, V. Y. Lee, R. D. Miller, S. Setayesh, K. Müllen, *Adv. Mater.* 2001, **13**, 1096-1099.
11 L.-C. Chi, W.-Y. Hung, H.-C. Chiu, K.-T. Wong, *Chem. Commun.* 2009, 3892-3894.
12 C. Poriel, J.-J. Liang, J. Rault-Berthelot, F. Barrière, N. Cocherel, A. M. Z. Slawin, D. Horhant, M. Virboul, G. Alcaraz, N. Audebrand, L. Vignau, N. Huby, G. Wantz, L. Hirsch, *Chem. Eur. J.* 2007, **13**, 10055-10069.
13 N. Cocherel, C. Poriel, L. Vignau, J.-F. Bergamini, J. Rault-Berthelot, *Org. Lett.* 2010, **12**, 452-455.
14 C. Poriel, N. Cocherel, J. Rault-Berthelot, L. Vignau, O. Jeannin, *Chem. Eur. J.* 2011, **17**, 12631-12645.
15 J. Jacob, L. Oldridge, J. Zhang, M. Gaal, E. J. W. List, A. C. Grimsdale, K. Müllen, *Curr. Appl. Phys.* 2004, **4**, 339-342.
16 K. H. Lee, S. O. Kim, J. N. You, S. Kang, J. Y. Lee, K. S. Yook, S. O. Jeon, J. Y. Lee, S. S. Yoon, *J. Mater. Chem.* 2012, **22**, 5145-5154.
17 S.-Y. Ku, L.-C. Chi, W.-Y. Hung, S.-W. Yang, T.-C. Tsai, K.-T. Wong, Y.-H. Chen, C.-I. Wu, *J. Mater. Chem.* 2009, **19**, 773-780.
18 T. Hadizad, J. Zhang, Z. Y. Wang, T. C. Gorjanc, C. Py, *Org. Lett.* 2005, **7**, 795-797.
19 D. Horhant, J.-J. Liang, M. Virboul, C. Poriel, G. Alcaraz, J. Rault-Berthelot, *Org. Lett.* 2006, **8**, 257-260.
20 W. Zhang, J. Smith, R. Hamilton, M. Heeney, J. Kirkpatrick, K. Song, S. E. Watkins, T. Anthopoulos, I. McCulloch, *J. Am. Chem. Soc.* 2009, **131**, 10814-10815.
21 H. Usta, C. Risko, Z. Wang, H. Huang, M. K. Deliomeroglu, A. Zhukhovitskiy, A. Facchetti, T. J. Marks, *J. Am. Chem. Soc.* 2009, **131**, 5586-5608.
22 D. T. Chase, A. G. Fix, S. J. Kang, B. D. Rose, C. Weber, Y. Zhong, L. Zakharov, M. C. Lonergan, C. Nuckolls, M. M. Haley, *J. Am. Chem. Soc.* 2012, **134**, 10349-1052.
23 H. Kim, N. Schulte, G. Zhou, K. Müllen, F. Laquai, *Adv. Mater.* 2011, **23**, 894-897.

24 Y.-I. Park, J. S. Lee, B. J. Kim, B. Kim, J. Lee, D. H. Kim, S.-Y. Oh, J. H. Cho, J.-W. Park, *Chem. Mater.* 2011, **23**, 4038-4044.
25 P. Sonar, L. Oldridge, A. C. Grimsdale, K. Müllen, M. Surin, R. Lazzaroni, P. Leclère, J. Pinto, L.-L. Chua, H. Sirringhaus, R. H. Friend, *Synth. Met.* 2010, 468-474.
26 H. Usta, A. Facchetti, T. J. Marks, *Acc. Chem. Res.* 2011, **44**, 501-510.
27 H. Usta, A. Facchetti, T. J. Marks, *J. Am. Chem. Soc.* 2008, **130**, 8580-8581.
28 H. Usta, A. Facchetti, T. J. Marks, *Org. Lett.* 2008, **10**, 1385-1388.
29 T. Hadizad, J. Zhang, D. Yan, Z. Y. Wang, J. P. M. Serbena, M. S. Meruvia, I. A. Hümmelgen, *J. Mater. Sci: Mater. Electron* 2007, **18**, 903-912.
30 S. Chaurasia, Y.-C. Chen, H.-H. Chou, Y. S. Wen, J. T. Lin, *Tetrahedron* 2012, **68**, 7755-7762.
31 J. Kim, S. H. Kim, I. H. Jung, E. Jeong, Y. Xia, S. Cho, I.-W. Hwang, K. Lee, H. Suh, H.-K. Shim, H. Y. Woo, *J. Mater. Chem.* 2010, **20**, 1577-1586.
32 Q. Zheng, B. J. Jung, J. Sun, H. E. Katz, *J. Am. Chem. Soc.* 2010, **132**, 5394-5404.
33 S. Chaurasia, C.-J. Liang, Y.-S. Yen, J. T. Lin, *J. Mater. Chem. C* 2015, **3**, 9765-9780.
34 Y. Shi, Q. Liu, G. Wu, L. Rong, J. Tang, *Tetrahedron* 2011, **67**, 1201-1209.
35 Y.-Y. Li, H.-Y. Lu, M. Li, X.-J. Li, C.-F. Chen, *J. Org. Chem.* 2014, **79**, 2139-2147.
36 M. Romain, D. Tondelier, B. Geffroy, O. Jeannin, E. Jacques, J. Rault-Berthelot, C. Poriel, *Chem. Eur. J.* 2015, **21**, 9426–9439.
37 D. Thirion, M. Romain, J. Rault-Berthelot, C. Poriel, *J. Mater. Chem.* 2012, **22**, 7149-7157.
38 C. Poriel, J. Rault-Berthelot, D. Thirion, F. Barrière, L. Vignau, *Chem. Eur. J.* 2011, **17**, 14031-14046.
39 B. Du, L. Wang, S.-C. Yuan, T. Lei, J. Pei, Y. Cao, *Polymer* 2013, **54**, 2935-2944.
40 A. G. Fix, P. E. Deal, C. L. Vonnegut, B. D. Rose, L. N. Zakharov, M. M. Haley, *Org. Lett.* 2013, **15**, 1362-1365.
41 A. Shimizu, Y. Tobe, *Angew. Chem. Int. Ed.* 2011, **50**, 6906-6910.
42 D. T. Chase, B. D. Rose, S. P. Mc Clintock, L. N. Zakharov, M. M. Haley, *Angew. Chem. Int. Ed.* 2011, **50**, 1127-1130.
43 A. Shimizu, R. Kishi, M. Nakano, D. Shiomi, K. Sato, T. Takui, I. Hisaki, M. Miyata, Y. Tobe, *Angew. Chem. Int. Ed.* 2013, **52**, 6076-6079.
44 K. H. Lee, S. O. Kim, S. Kang, J. Y. Lee, K. S. Yook, J.-Y. Lee, S. S. Yoon, *Eur. J. Org. Chem.* 2012, 2748-2755.
45 M. Romain, M. Chevrier, S. Bebiche, T. Mohammed-Brahim, J. Rault-Berthelot, E. Jacques, C. Poriel, *J. Mater. Chem. C* 2015, **3**, 5742-5753.
46 C. Poriel, R. Métivier, J. Rault-Berthelot, D. Thirion, F. Barrière, O. Jeannin, *Chem. Commun.* 2011, **47**, 11703-11705.
47 C.-Y. Chan, Y.-C. Wong, M.-Y. Chan, S.-H. Cheung, S.-K. So, V. W.-W. Yam, *Chem. Mater.* 2014, **26**, 6585-6594.
48 L. Yao, S. Sun, S. Xue, S. Zhang, X. Wu, H. Zhang, Y. Pan, C. Gu, F. Li, Y. Ma, *J. Phys. Chem. C* 2013, 14189-14196.
49 M. Romain, D. Tondelier, B. Geffroy, A. Shirinskaya, O. Jeannin, J. Rault-Berthelot, C. Poriel, *Chem. Commun.* 2015, **51**, 1313-1315.
50 M. Romain, D. Tondelier, O. Jeannin, B. Geffroy, J. Rault-Berthelot, C. Poriel, *J. Mater. Chem. C* 2015, **3**, 9701-97014.
51 Q. Zhang, J. Li, K. Shizu, S. Y. Huang, S. Hirata, H. Miyazaki, C. Adachi, *J. Am. Chem. Soc.* 2012, **134**, 14706-14709.

52 H. Li, A. S. Batsanov, K. C. Moss, H. L. Vaughan, F. B. Dias, K. T. Kamtekar, M. R. Bryce, A. P. Monkman, *Chem. Commun.* 2010, **46**, 4812-4814.
53 Y. Li, Z. Wang, X. Li, G. Xie, D. Chen, Y.-F. Wang, C.-C. Lo, J. Peng, Y. Cao, S.-J. Su, *Chem. Mater.* 2015, **27**, 1100-1109.
54 S.-J. Kim, J. Leroy, C. Zuniga, Y. Zhang, L. Zhu, J. S. Sears, S. Barlow, J. L. Brédas, S. R. Marder, B. Kippelen, *Org. Electron.* 2011, **12**, 1314-1318.
55 F.-M. Hsu, C.-H. Chien, Y.-J. Hsieh, C.-H. Wu, C.-F. Shu, S.-W. Liu, C.-T. Chen, *J. Mater. Chem.* 2009, **19**, 8002-8008.
56 H. Sasabe, Y. Seino, M. Kimura, J. Kido, *Chem. Mater.* 2012, **24**, 1404-1406.
57 M. P. Gaj, C. Fuentes-Hernandez, Y. Zhang, S. R. Marder, B. Kippelen, *Org. Electron.* 2015, **16**, 109-112.
58 D. Thirion, C. Poriel, J. Rault-Berthelot, F. Barrière, O. Jeannin, *Chem. Eur. J.* 2010, **16**, 13646-13658.
59 A. Bondi, *J. Phys. Chem.* 1964, **68**, 441-451.
60 S. Thiery, D. Tondelier, C. Declairieux, G. Seo, B. Geffroy, O. Jeannin, J. Rault-Berthelot, R. Métivier, C. Poriel, *J. Mater. Chem. C* 2014, **2**, 4156-4166.
61 S. Merlet, M. Birau, Z. Y. Wang, *Org. Lett.* 2002, **4**, 2157-2159.
62 A. P. Kulkarni, C. J. Tonzola, A. Babel, S. A. Jenekhe, *Chem. Mater.* 2004, **16**, 4556-4573.
63 S. Thiery, D. Tondelier, C. Declairieux, B. Geffroy, O. Jeannin, R. Métivier, J. Rault-Berthelot, C. Poriel, *J. Phys. Chem. C* 2015, **119**, 5790–5805.
64 J. H. Seo, N. S. Han, H. S. Shim, J. H. Kwon, J. K. Song, *Bull. Korean Chem. Soc.* 2011, **32**, 1415.
65 E. Baranoff, B. F. E. Curchod, *Dalton Trans.* 2015, **44**, 8318-8329.
66 K. S. Yook, J. Y. Lee, *Adv. Mater.* 2012, **24**, 3169-3190.
67 N. S. Han, S. H. Sohn, S. M. Park, J. K. Song, *Bull. Korean Chem. Soc.* 2013, **34**, 1547-1550.
68 Y. Fukuda, T. Watanabe, T. Wakimoto, S. Miyaguchi, M. Tsuchida, *Synt. Met*. 2000, **111-112**, 1-6.
69 *C. Fery, S. Cina, H. Doyeux, B. Geffroy, C. Denis, P. Maisse, MRS Proceedings* 2005*, 871, I9.13*.

Table of Contents

We report herein the synthesis, structural, electrochemical and photophysical properties of two semi-conductors based on dihydroindeno[2,1-*b*]-fluorene scaffold incorporating either thioxanthene units or dioxothioxanthene units. The incorporation as host material in green and blue PhOLEDs has been finally realized.